Quadrupole moments of high spin isomers in ^{213}Fr, ^{212}Fr, and ^{211}Fr

F. Hardeman, G. Neyens, G. Scheveneels, R. Nouwen, G. S'heeren, M. Van Den Bergh, and R. Coussement
Instituut voor Kern- en Stralingsfysika, Katholieke Universiteit Leuven, B-3001 Leuven, Belgium

A. P. Byrne,* R. Müsseler, H. Hübel, and G. Baldsiefen
Institut für Strahlen- und Kernphysik, Universität Bonn, Nussallee 14-16, D-5300 Bonn 1, West Germany
(Received 20 June 1990)

The level mixing spectroscopy method has been applied to measure the static quadrupole moments of six isomeric states in ^{213}Fr, ^{212}Fr, and ^{211}Fr ($Z=87$). For isomers with the proton configuration $\pi h^4_{9/2} i_{13/2}$ a large increase of the quadrupole moment was observed with the removal of neutrons from the closed $N=126$ core: $Q(\frac{29}{2}^+, ^{213}\text{Fr}) = -70(7)$ e fm^2, $Q(15^-, ^{212}\text{Fr}) = -80(12)$ e fm^2, and $Q(\frac{29}{2}^+, ^{211}\text{Fr}) = -107(18)$ e fm^2. Quadrupole moments for very high spin states were also measured: $Q(\frac{65}{2}^-, ^{213}\text{Fr}) = -219(53)$ e fm^2, $Q(27^-, ^{212}\text{Fr}) = -152(31)$ e fm^2, and $Q(\frac{45}{2}^-, ^{211}\text{Fr}) = -198(56)$ e fm^2. The observed values are in good agreement with shell-model calculations, but are lower than that predicted using the deformed-independent particle model. The implantation behavior of Fr in a Tl host is also discussed.

I. INTRODUCTION

Isotopes close to doubly magic nuclei like ^{208}Pb are characterized by the occurrence of many isomeric levels: This permits the direct measurement of quadrupole moments using hyperfine methods like time-differential perturbed angular distribution[1] (TDPAD) or level mixing spectroscopy[2] (LEMS). One interest in such experiments is to see whether the spherical shape of the doubly magic nuclei is maintained when valence particles or holes are added. In the lead region systematic studies have been performed for the isotopes of Pb ($Z=82$) (e.g., 12^+ isomers),[3,4] Bi ($Z=83$),[5] Po ($Z=84$),[6,7] At ($Z=85$),[8,9] and Rn ($Z=86$).[10,11] However, the behavior at high spin is not yet firmly established. In particular, the quadrupole moment for the $\frac{63}{2}^-$ state in ^{211}Rn is much lower than that predicted by the deformed-independent particle model (DIPM).[11]

The spectroscopic information of the Fr isomers[12] was recently extended to higher energies and spins with an isomer of spin $\frac{65}{2}^-$ and lifetime 4 μs identified for the ^{213}Fr ($Z=87$, $N=126$) isotope.[13] The long mean life and high spin of this isomer precludes a quadrupole moment measurement using the TDPAD technique. However, as the LEMS method is virtually independent of the spin (for $I > 10\hbar$) and is an integral technique, the static quadrupole moment is measurable for this isomer.

In addition to the $\frac{65}{2}^-$ isomer, several other isomers suitable for quadrupole moment determination[12,13] have been observed in the isotopes ^{213,212,211}Fr. The properties

TABLE I. Experimental properties of states.

Isotope	I^π	τ	Main configuration	g[a]	Transition energy[b] (keV)
^{213}Fr	$\frac{21}{2}^-$	720 ns	$\pi h^5_{9/2}$	0.888(3)	1189($E2$)
	$\frac{29}{2}^+$	350 ns	$\pi h^4_{9/2} i_{13/2}$	1.055(5)	681($E3$)
	$\frac{65}{2}^-$	4.5 μs	$\pi h^3_{9/2} i^2_{13/2} \nu p^{-2}_{1/2} g_{9/2} i_{11/2}$	0.695(7)	1259($E3$)
^{212}Fr	11^+	39 μs	$\pi h^5_{9/2} \nu p^{-1}_{1/2}$	0.9899(4)	542($E2$)
					847($E2$)
	15^-	870 ns	$\pi h^4_{9/2} i_{13/2} \nu p^{-1}_{1/2}$	1.043(8)	612($E3$)
	27^-	450 ns	$\pi h^3_{9/2} i^2_{13/2} \nu p^{-2}_{1/2} g_{9/2}$	0.81(1)	588($E3$)
^{211}Fr	$\frac{29}{2}^+$	210 ns	$\pi h^4_{9/2} i_{13/2} \nu p^{-2}_{1/2}$	1.06(1)	800($E2$)
					653($E2$)
	$\frac{45}{2}^-$	178 ns	$\pi h^3_{9/2} i^2_{13/2} \nu p^{-2}_{1/2}$	1.08(1)	728($E3$)

[a]From Refs. 12 and 13.
[b]Gamma-ray transition energy for which LEMS curve was obtained. The multipolarity is shown in brackets.

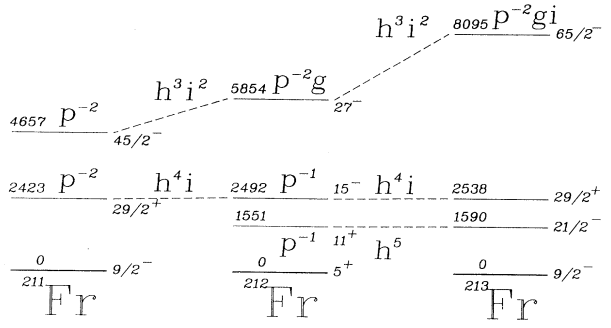

FIG. 1. Partial-level schemes of the isomer ^{211}Fr, ^{212}Fr, and ^{213}Fr. The relationships between levels is indicated, with the principal proton configuration shown as the dashed lines and the neutron configuration at each level.

of these levels are given in Table I, and the relationship between groups of isomers is indicated in Fig. 1. While the quadrupole moments of the very high spin isomers are of particular interest, quadrupole moments for the other states are also of value. The lowest isomers in the ^{213}Fr and ^{212}Fr isotopes (the $\frac{21}{2}^-$ and 11^+ states) occur because of the half-filling of the $\pi h_{9/2}$ shell. For the pure $\pi h^5_{9/2}$ configuration, the shell model predicts a zero quadrupole moment, so that any measured moment for these states reflects the degree of admixture in these configurations. The isomers with the common proton configuration $\pi h^4_{9/2} i_{13/2}$ are closely related to similar isomers in the At isotopes,[8] with the common $\pi h^2_{9/2} i_{13/2}$ configuration, for which a large increase in quadrupole moment has been observed with the removal of neutrons from the $N=126$ core. It is of interest to determine whether the Fr isotopes show similar behavior.

This paper reports on the results of a series of measurements of quadrupole moments obtained using the LEMS technique. Parallel measurements were also performed using the TDPAD technique, and these results have been published elsewhere.[15]

II. EXPERIMENTS

A. Level mixing spectroscopy method

The LEMS method for the determination of quadrupole moments is a relatively new technique. However, it has been applied successfully to the measurement of the Bi (Ref. 5) and At (Ref. 9) isotopes. As the technique is described extensively in Refs. 2 and 14, we restrict the discussion here to a summary of the basic technique and aspects particular to the Fr experiments.

The experimental arrangement is indicated in Fig. 2. The beam is incident on a single noncubic crystal which has been mounted so that the electric-field-gradient (EFG) axis is misaligned with the beam axis by a large angle β. An external magnetic field is applied along the beam axis, and the combined magnetic and quadrupole interactions perturb the initial nuclear orientation, which is then observed via the detection of the time-integrated angular distribution as a function of the magnetic field.

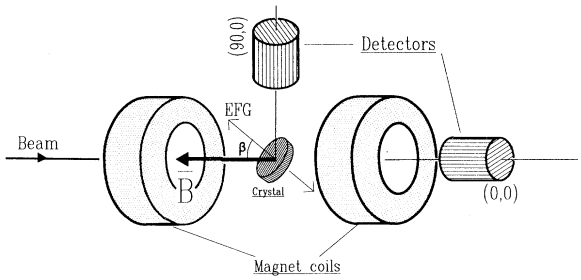

FIG. 2. Experimental setup for the LEMS experiments.

Calculated curves as a function of magnetic field and misalignment angle β, for a state with $I=10$, are shown in Fig. 3(a). Three different regimes occur: (i) At zero magnetic field and for $\beta \neq 0$, the initial anisotropy is reduced due to the quadrupole interaction. (ii) At high fields the quadrupole interaction is decoupled from the

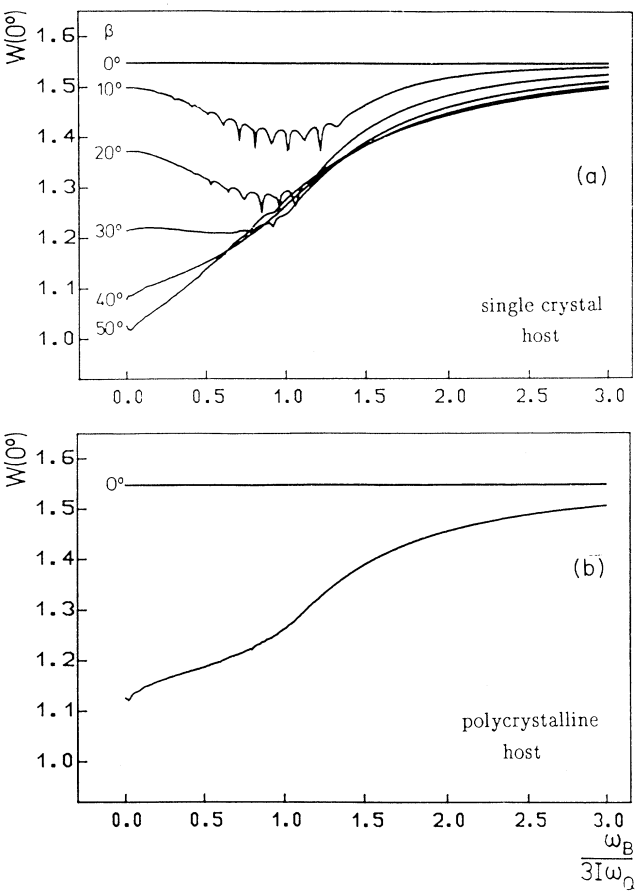

FIG. 3. Numerical calculations of LEMS curves for spin $I=10$ plotted as a function of the ratio of the magnetic and quadrupole interaction frequencies. $\omega_B = g\mu_N B/\hbar$ and $\omega_Q = eQV_{zz}/\hbar 4I(2I-1)$. (a) shows the curves for a single crystal as a function of β (see Fig. 2). (b) shows the equivalent curve for a polycrystalline host. The curves for higher spins are almost identical to those shown.

magnetic one, which induces a Larmor precession round the field (beam) axis. As the field axis is a symmetry axis of the initial orientation, the observed anisotropy reflects the orientation induced by the nuclear reaction, and a saturationlike behavior of the anisotropy as a function of the magnetic field B is found. (iii) In the intermediate-field range, a mixing of many hyperfine levels takes place. The shape of the resultant curve depends on the ratio of the product of the quadrupole moment and field gradient strength to the g factor, and may be calculated numerically.[2,14] Like the TDPAD method, the technique is not sensitive to the sign of the quadrupole moment, and only magnitudes may be determined.

The method is not restricted to single-crystal hosts, and polycrystalline materials may also be used. In these cases an integration must be performed over all angles β, and the equivalent curve for a polycrystalline host is shown in Fig. 3(b).

B. Experimental details

In all experiments states in francium nuclei were populated using a carbon-induced xn reaction on thick thallium metal targets. Both single and polycrystalline targets were used, with the Tl providing both target and host material (Tl is hexagonal at temperatures below 503 K). While in the majority of the experiments we used natural Tl material (65% ^{205}Tl, 35% ^{203}Tl), additional selectivity was also obtained with experiments on samples enriched to over 90% in ^{203}Tl (for ^{211}Fr) or ^{205}Tl (for ^{212}Fr and ^{213}Fr). Experiments were performed both at elevated temperature 400 K and near liquid-He temperature 6 K. Beams of ^{12}C and ^{13}C with energies of 85 and 90 MeV were obtained from the cyclotron "Cyclone" of the Université Catholique de Louvain at Louvain-la-Neuve (Belgium). Although not required for the LEMS technique, pulsed beams were used to improve the quality of the collected data by allowing selection of events following isomeric decays.

Gamma rays were detected in three HP Ge detectors, with two of them positioned at 90° to the beam axis and the third at 0°. Use of the ratio $N(0°)/N(90°)$ avoids problems of normalization for different magnetic-field values. A list of gamma rays used in the analysis is given in Table I. Where possible, $E3$ transitions were chosen in order to maximize the observed anisotropy. Gamma-ray intensities were extracted by fitting a Gaussian shape including tails of the photopeak. Peak shape parameters were obtained by fits to photopeaks from daughter activities and from calibration spectra taken before and after each run.

The external magnetic field was produced by a superconducting magnet, and fields up to 5 T were used. Corrections due to the modification of the external magnetic field by Knight shift and diamagnetic effects were applied.[13]

III. RESULTS

A. Radiation damage effects

In previous LEMS experiments,[2,5,9,14] the LEMS curves $N(0°)/N(90°)$ as a function of magnetic field B were analyzed by fitting a theoretical curve, dependent on three free parameters: the relative detection efficiency, the initial orientation (fitted by assuming a Gaussian distribution of the population of the $|m\rangle$ states yielding only one fit parameter), and the quadrupole interaction strength. In the present series of measurements, the curves (see Fig. 4) could not be fitted in the same manner. The shape of the curves indicated the presence of an additional electric-field gradient, and the subsequent analysis required the inclusion of two more fit parameters: the relative population of both sites and the magnitude of the second interaction frequency.

Further evidence for the occurrence of more than one site was found in an experiment using a single crystal of natural thallium. Initially, the c axis of this crystal was put parallel to the beam (and magnetic-field) axis. For an electric-field gradient originating from a substitutional lattice site position, this corresponds to $\beta=0°$ [see Fig. 3(a)] and causes a constant contribution to the anisotropy when measured as a function of the magnetic field. The experimental curve for this measurement is shown in Fig. 5 and clearly shows that the larger electric-field gradient observed in the present work has a symmetry different from that of the lattice symmetry. When the crystal was rotated so that $\beta=40°$, both field gradients were again present, demonstrating that the occurrence of multiple sites was not related to sample preparation or surface effects, but to microscopic phenomena. Additional support for this interpretation was given by the results from the TDPAD measurements,[15] which also indicated the presence of different electric-field gradients. The interpretation of these results is discussed below.

B. Quadrupole moments of the Fr isomers

A selection of LEMS curves from the current set of experiments is given in Fig. 4, and the interaction frequencies obtained are given in Table II. In order to extract absolute quadrupole moments, a calibration of the electric-field gradient for FrTl is required. Following Ref. 15, we have adopted the calculated value of $Q(\frac{29}{2}^+, {}^{213}\mathrm{Fr}) = -70(7)\ e\,\mathrm{fm}^2$ for a calibration, and absolute quadrupole moments for states measured here are given in Table II.

Data for the $\frac{21}{2}^-$ isomer in ^{213}Fr and the 11^+ state in ^{212}Fr were also obtained in the present series of experiments. As their main configuration is $h^5_{9/2}$, presenting a half-closed shell, very small quadrupole moments are to be expected, with the departure from zero being induced by configuration impurities. However, due to this fact as well as to the presence of several sites and the feeding from higher-lying isomers, it was difficult to extract accurate results from the present data, and a quadrupole moment of $\simeq 10\ e\,\mathrm{fm}^2$ was obtained for these states. (Additional measurements at lower bombarding energies would be required to reliably extract more accurate values.)

IV. DISCUSSION

A. Implantation behavior

The adoption of a calibration quadrupole moment for one of the states measured allows the determination of

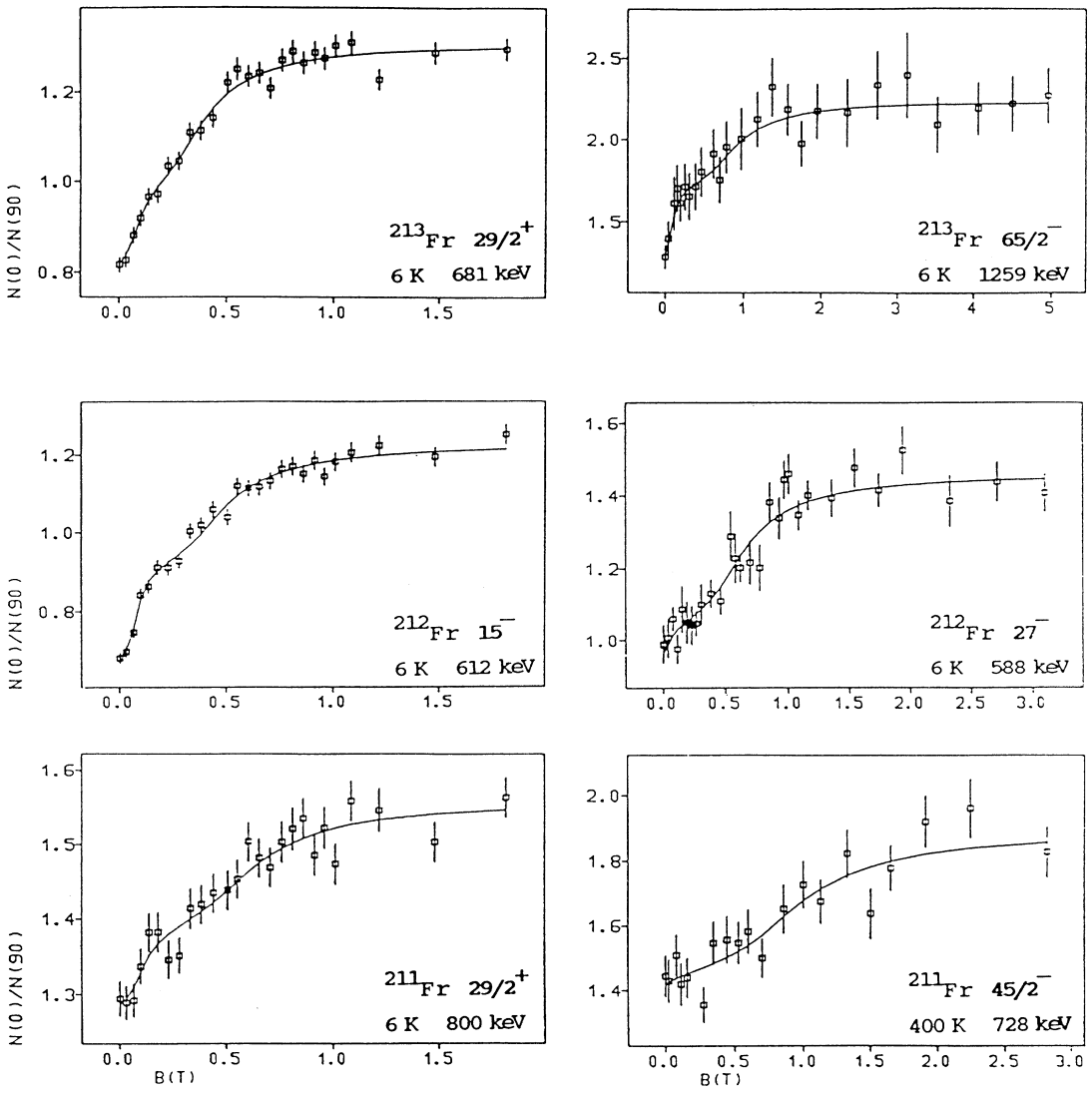

FIG. 4. Selection of LEMS curves obtained in the present work. The curve for the ^{211}Fr, 728-keV line was obtained using a single crystal oriented with $\beta=0°$ and, consequently, shows only a single interaction frequency (see text).

the electric-field gradients V_{zz} observed in the present work, and these values are given in Table III. In the extraction of the quadrupole moments, the larger interaction frequency has been used, and the lower EFG is only poorly determined in the present work. The parallel TDPAD study[15] also observed several interaction frequencies, with electric-field gradients of $V_{zz}\simeq 0.5\times 10^{17}$ and 1.7×10^{17} V cm^{-2} measured. A third interaction frequency was also observed in the TDPAD study with the EFG $V_{zz}\sim 5\times 10^{17}$ V cm^{-2} comparable to that observed in the LEMS measurement. This field gradient has been associated with nearest-neighbor vacancies.[15] The variety of interaction frequencies observed can be attributed to the very large difference in size between the Fr atom and those of the host (the ratio of radii is 1.85). This mismatch is likely to result in a perturbation of the lattice, and a strong attraction to vacancies is probable.

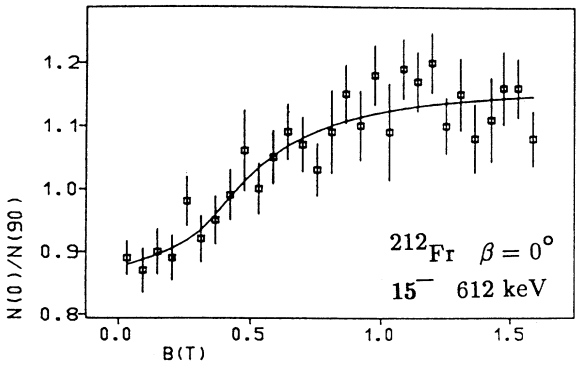

FIG. 5. LEMS curves for the ^{212}Fr, 612-keV transition obtained with a single crystal oriented with $\beta=0°$. A single (defect) interaction frequency is observed.

TABLE II. Quadrupole moments in the Fr isotopes.

Isotope	Isomer	ν_{Q_d} [a] (MHz) (6 K)	ν_{Q_d} [a] (MHz) (400 K)	$\frac{Q_i}{Q(\frac{29}{2}^+)}$ [b]	Q_{expt} [c] (e fm^2)	Q_{expt} [d] (e fm^2)	Q_{calc} [e] (e fm^2)
^{213}Fr	$\frac{29}{2}^+$	85(10)	115(15)	1.0	−70(7)	−70(7)	
	$\frac{65}{2}^-$	275(60)	325(150)	3.13(69)	−219(53)		−239
^{212}Fr	15^-	105(10)	120(15)	1.14(13)	−80(12)	−84(13)	−86
	27^-	185(25)		2.18(39)	−152(31)	−174(33)	−208
^{211}Fr	$\frac{29}{2}^+$	125(15)	190(30)	1.53(20)	−107(18)		−106
	$\frac{45}{2}^-$		325(75)	2.83(75)	−198(56)		−190

[a] $\nu_{Q_d} = eQV_{zz}/h$ second interaction frequency.

[b] Ratios of the experimental interaction frequencies for particular states compared to the ^{213}Fr, $\frac{29}{2}^+$ interaction frequency. A weighted mean of the 6 and 400 K has been taken.

[c] Quadrupole moments obtained in the present work assuming $Q(^{213}\text{Fr}, \frac{29}{2}^+) = -70(7)$ and assuming negative values throughout.

[d] Experimental value from TDPAD measurement (Ref. 15).

[e] Calculated values using effective charges and octupole coupled shell-model configurations (see text).

Similar incomplete substitutional fractions have been observed for Fr in Fe systems in nuclear orientation experiments in the mK region,[16] and substitutional fractions of 40% have been observed for Cs and Rb (belonging to the Fr group) in Fe and V hosts.[17–19]

B. Calculation of quadrupole moments

One of the most successful approaches to the calculation of the properties of levels in the translead region has been the use of the semiempirical shell model, in which properties of complex states are expressed in terms of simple components. This method is of limited application in the calculation of quadrupole moments since very few independent measurements of quadrupole moments are available. Calculated values are available.[20,21] However, these values fail to reproduce the quadrupole moments of many simple configurations, particularly those involving the $\pi i_{13/2}$ orbital. The use of effective charges has also been considered in the lead region.[22] However, this technique is only useful if one considers an expanded configuration space which includes the octupole contribution explicitly.[15] Using the proton effective charge of 1.5e, derived from states in the Bi, Po, and At isotopes, we have calculated the quadrupole moment of the $\frac{29}{2}^+$ state in ^{213}Fr as $Q(\frac{29}{2}^+, ^{213}\text{Fr}) = -70(7)$ e fm^2. In this calculation we adopted the wave function of Ref. 12, and we used the empirical values for the $Q(\pi h^4_{9/2}, ^{212}\text{Rn})$ (Ref. 23) and $Q(3^-, ^{208}\text{Pb})$ (Ref. 24) moments, and the mean-square radii as tabulated by Sagawa and Arima.[21] The error of 7 e fm^2 has been assigned to accommodate the discrepancy between the measured value for $Q(\pi h^4_{9/2})$ and that calculated using realistic shell-model wave functions.[15]

TABLE III. Results for the EFG of Fr in Tl obtained with LEMS.

T (K)	V_{zz1} [a] (10^{17} V/cm^2)	F_1 (%)	V_{zz2} [b] (10^{17} V/cm^2)	F_2 (%)
400	0.6(4)	45(5)	6.8(11)	55(5)
6	1.0(2)	46(3)	5.0(8)	54(3)

[a] Deduced electric-field gradient for lowest interaction frequency measured for the ^{213}Fr, $\frac{29}{2}^+$ state.

[b] Deduced electric-field gradient for the larger interaction frequency.

C. Variation of quadrupole moments with neutron number

The proton effective charge used above is only appropriate for the $N=126$ core. In Fig. 6 the variation of

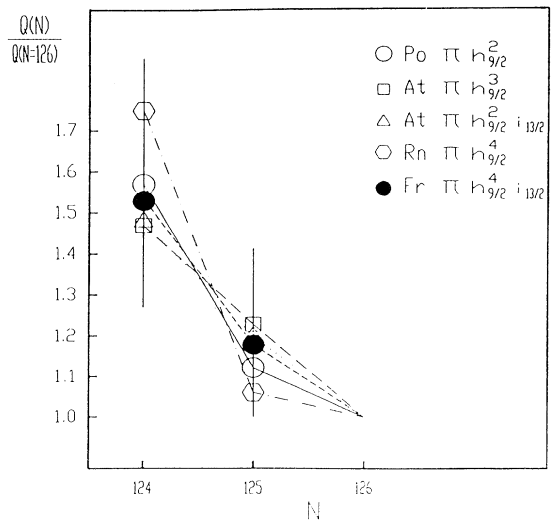

FIG. 6. Systematics of the quadrupole moments as a function of neutron number for simple configurations.

the quadrupole moment as a function of the neutron number is plotted, for both the $\pi h_{9/2}^4 i_{13/2}$ states measured here and other related states in the lighter isotones.[6–8,10,23] This figure shows that the same change in quadrupole moment occurs for all these configurations, clearly showing a softening of the core when $p_{1/2}$ neutrons are removed. This can be explained from the Nilsson diagrams for the $\nu p_{1/2}$ orbital.[25] The energy increases drastically as a function of the deformation parameter, indicating the large contribution of the $p_{1/2}$ neutrons to the sphericity of the core. This removal implies a softening of the core and an increase in the quadrupole moment.

In order to calculate the quadrupole moments for the states measured in the Fr nuclei, we have extracted proton effective charges from the available data for the Bi, Po, and At isotopes of $e_{\text{eff}}=1.85e$ and $2.28e$ for the $N=125$ and 124 cores, respectively.

D. Quadrupole moments of the 27^- and $\frac{65}{2}^-$ states

The 27^- and $\frac{65}{2}^-$ states in ^{212}Fr and ^{213}Fr, respectively, are of particular interest since the role of deformation, if any, in the formation of these highly aligned, core-excited states has not yet been established. Previous measurements for a related state in ^{211}Rn, the $\frac{63}{2}^-$ state with the dominant configuration $\pi(h_{9/2}^2 i_{13/2}^2)\nu(f_{5/2}^{-1} g_{9/2} i_{11/2})$, obtained a quadrupole moment[11] of $-160(22)$ e fm^2, considerably lower than that predicted by the DIPM.[26,27]

The most successful description of the high spin isomers in this region is that they arise because of the coupling between single-particle states and the octupole 3^- vibrational state. The many-particle octupole coupling model (MPOC) has been able to reproduce well both the excitation energies and transition strengths from these isomers (see Refs. 13 and 28, and references therein). Detailed wave functions from this model for the $\frac{65}{2}^-$, ^{213}Fr state are given in Ref. 13 and for the 27^- state in Ref. 15. Since there is only a relatively small variation in quadrupole moments for particular valence nucleons, the calculated quadrupole moments for these states are not very sensitive to the details of the wave functions. This may be seen by comparing the quadrupole moments calculated for the largest single component of the wave function (typical amplitudes, 55%), $Q(\pi h_{9/2}^3 i_{13/2}^2 \nu p_{1/2}^{-2} g_{9/2}) = -216$ e fm^2 and $Q(\pi h_{9/2}^3 i_{13/2}^2 \nu p_0^{-2} g_{9/2} i_{11/2}) = -242$ e fm^2, with the values calculated for the full wave function $Q(27^-,\ ^{212}\text{Fr}) = -208$ e fm^2 and $Q(\frac{65}{2}^-,\ ^{113}\text{Fr}) = -239$ e fm^2, respectively.

The agreement between the measured and calculated values is quite good, although both calculations appear to slightly overestimate the observed values. It should be pointed out that an $N=124$ core, hence a proton effective charge of $e_{\text{eff}}=2.28e$, has been used for both the 27^- and $\frac{65}{2}^-$ calculations since both involve the removal of two neutrons from the $N=126$ core. However, it is not clear whether the extra valence neutrons might modify the effective charge. (A value of $0.9e$ has been used for the neutron effective charge.) The present data do appear to be lower than the calculated values; however, the large errors make such evaluations difficult to substantiate.

An alternative model, the DIPM, has been used to describe the formation of yrast isomers in the lead region.[27] While in broad terms the model does predict the occurrence of yrast traps, it fails to predict the correct configurations; nor can it explain the enhanced $E3$ transitions deexciting most of the isomeric states in the region. One prediction of the DIPM is that the very high spin isomers should have a significant deformation. While no calculations have been performed for the Fr isotopes, it is expected that the deformation calculated for the $\frac{63}{2}^-$ state in ^{212}Rn ($\beta=0.1$) (Ref. 11) should be very similar to the deformation for the 27^- and $\frac{65}{2}^-$ states. Such deformations correspond to quadrupole moments in excess of -300 e fm^2, which are significantly above the measured values, further questioning the applicability of this model to the high spin isomers in this region.

V. CONCLUSIONS

The quadrupole moments of six isomers in the nuclei ^{211}Fr, ^{212}Fr, and ^{213}Fr have been measured. The trend of rising quadrupole moment with removal of neutrons from the $N=126$ core observed for previous translead nuclei is supported by the Fr results.

The quadrupole moments measured for the very high spin states in the Fr nuclei agree with those predicted by the shell model, but do not support the assertion that isomerism in this region is a result of a gain in deformation energy.

The present series of experiments also demonstrates the successful application of the LEMS technique to the measurement of isomeric states not easily accessible by other methods.

ACKNOWLEDGMENTS

We would like to thank the staff of the Louvain-la-Neuve Cyclone facility for their assistance during the course of this work. One of us (A.P.B.) gratefully acknowledges support from the Alexander von Humboldt Stiftung. This work was supported in part by the BMFT of the Federal Republic of Germany.

*Present address: Department of Nuclear Physics, The Australian National University, P.O. Box 4, Canberra 2601, Australia.

[1] R. M. Steffen and K. Alder, in *The Electromagnetic Interaction in Nuclear Spectroscopy*, edited by W. D. Hamilton (North-Holland, Amsterdam, 1975), p. 583.

[2] F. Hardeman, G. Scheveneels, G. Neyens, R. Nouwen, G. S'heeren, M. Van Den Bergh, and R. Coussement, Phys. Rev. C (to be published); G. Scheveneels, F. Hardeman, G. Neyens, and R. Coussement, Hyperfine Interact. **52**, 257 (1989).

[3] H.-E. Mahnke, T. K. Alexander, H. R. Andrews, O. Hausser,

P. Tarus, D. Ward, E. Dafni, and G. D. Sprouse, Phys. Lett. **88B**, 48 (1979).
[4]S. Zywietz, H. Grawe, H. Haas, and M. Menningen, Hyperfine Interact. **9**, 109 (1981).
[5]G. Scheveneels, F. Hardeman, G. Neyens, and R. Coussement (submitted to Phys. Rev. C).
[6]E. Dafni, M. H. Rafailovich, T. Marshall, G. Schatz, and G. D. Sprouse, Nucl. Phys. **A394**, 245 (1983).
[7]H.-E. Mahnke, H. Haas, W. Semmler, R. Sielemann, and W. D. Zeitz, Z. Phys. B **45**, 203 (1982).
[8]H.-E. Mahnke, W. Semmler, H. Grawe, H. Haas, and R. Sielemann, Phys. Lett. B **122**, 27 (1983).
[9]G. Scheveneels, F. Hardeman, G. Neyens, and R. Coussement (submitted to Phys. Rev. C).
[10]A. Berger, H. Grawe, H.-E. Mahnke, E. Dafni, M. Hass, E. Naim, and M.-H. Rafailovich, Phys. Lett. B **182**, 11 (1986).
[11]E. Dafni, M. Hass, E. Naim, M.-H. Rafailovich, A. Berger, H. Grawe, and H.-E. Mahnke, Phys. Rev. Lett. **55**, 1269 (1985).
[12]A. P. Byrne, G. D. Dracoulis, C. Fahlander, H. Hübel, A. R. Poletti, A. E. Stuchbery, J. Gerl, R. F. Davie, and S. J. Poletti, Nucl. Phys. **A448**, 137 (1986).
[13]A. P. Byrne, R. Müsseler, H. Hübel, M. Murzel, K. Theine, W. Schmitz, K. H. Maier, H. Kluge, H. Grawe, and H. Haas, Phys. Rev. B **217**, 38 (1989).
[14]F. Hardeman, G. Scheveneels, G. Neyens, R. Nouwen, and R. Coussement, invited paper of the VIIIth International Conference on Hyperfine Interactions, Prague, 1989 [Hyperfine Interact. **59**, 13 (1990)].
[15]A. P. Byrne, R. M. Müsseler, H. Hübel, K. H. Maier, and H. Kluge, Nucl. Phys. **A516**, 145 (1990).
[16]J. Wouters, N. Severijns, J. Vanhaverbeke, W. Vanderpoorten, and L. Vanneste, contribution to the VIIIth International Conference on Hyperfine Interactions, Prague, 1989 [Hyperfine Interact. **61**, 1391 (1990)].
[17]O. Meyer and A. Turos, Nucl. Instrum. Methods Phys. Rev. B **19/20**, 136 (1987).
[18]A. Turos, A. Azzam, M. K. Kloska, and O. Meyer, Nucl. Instrum. Methods Phys. Rev. B **19/20**, 123 (1987).
[19]M. K. Kloska and O. Meyer, Nucl. Instrum. Methods Phys. Rev. B **19/20**, 140 (1987).
[20]J. Speth, E. Werner, and W. Wild, Phys. Rep. C **33**, 127 (1977); P. Ring, R. Bauer, and J. Speth, Nucl. Phys. **A206**, 97 (1973).
[21]H. Sagawa and A. Arima, Phys. Lett. B **202**, 15 (1988).
[22]G. Astner, I. Bergström, J. Blonqvist, B. Fant, and K. Wikström, Nucl. Phys. **A182**, 219 (1972).
[23]E. Dafni, M. Hass, E. Naim, M. H. Rafailovich, A. Berger, H. Grawe, and H.-E. Mahnke, Nucl. Phys. **A441**, 501 (1985).
[24]R. H. Spear, W. J. Vermeer, M. T. Esat, J. A. Keuhner, A. M. Baxter, and S. Hinds, Phys. Lett. **128B**, 29 (1983).
[25]For example, *Table of Isotopes*, edited by C. M. Lederer and V. S. Shirley (Wiley, New York, 1978), Appendix 6.
[26]G. Anderson, S. F. Larsson, G. Leander, J. Dudek, B. Nerlo-Pomorska, K. Pomorski, and Z. Szymanski, Nucl. Phys. **A268**, 205 (1976).
[27]K. Matsuyanagi, T. Døssing, and K. Neergard, Nucl. Phys. **A307**, 253 (1978).
[28]S. J. Poletti, G. D. Dracoulis, A. R. Poletti, A. P. Byrne, A. E. Stuchbery, and J. Gerl, Nucl. Phys. **A448**, 189 (1986).